Optics Letters

Atmospheric tomography for artificial satellite observations with a single guide star

Michael Hart,[1,2,*] Stuart M. Jefferies,[3,2] and Douglas A. Hope[4]

[1]College of Optical Sciences, University of Arizona, Tucson, Arizona 85721, USA
[2]Institute for Astronomy, University of Hawai'i, 34 'Ohia Ku Street, Pukalani, Hawaii 96768, USA
[3]Department of Physics and Astronomy, Georgia State University, Atlanta, Georgia 30303, USA
[4]Center for Space Situational Awareness Research, U.S. Air Force Academy, Colorado Springs, Colorado 80848, USA
*Corresponding author: mhart@optics.arizona.edu

Received 1 June 2016; accepted 14 July 2016; posted 20 July 2016 (Doc. ID 267411); published 3 August 2016

Estimation of wavefront errors in three dimensions is required to mitigate isoplanatic errors when using adaptive optics or numerical restoration algorithms to recover high-resolution images from blurred data taken through atmospheric turbulence. Present techniques rely on multiple beacons, either natural stars or laser guide stars, to probe the atmospheric aberration along different lines of sight, followed by tomographic projection of the measurements. In this Letter, we show that a three-dimensional estimate of the wavefront aberration can be recovered from measurements by a single guide star in the case where the aberration is stratified, provided that the telescope tracks across the sky with nonuniform angular velocity. This is generally the case for observations of artificial Earth-orbiting satellites, and the new method is likely to find application in ground-based telescopes used for space situational awareness.

OCIS codes: (010.1285) Atmospheric correction; (010.1330) Atmospheric turbulence; (010.7350) Wave-front sensing.

http://dx.doi.org/10.1364/OL.41.003723

The three-dimensional nature of the atmosphere imposes anisoplanatic effects on ground-based telescopes designed to deliver high-resolution imaging. Turbulence broadly distributed along the line of sight introduces angular anisoplanatism, a strong field dependence in the point-spread function. Adaptive optics (AO) systems that rely on a laser guide star (LGS) are additionally subject to focal anisoplanatism arising because the volume of air sampled by the beacon at finite range differs from that encountered by a more distant object. To achieve unaberrated imagery in either case, the wavefront must first be characterized over the volume of atmosphere between the scene and the telescope.

In nighttime astronomy, this is achieved by wavefront sensor (WFS) measurements of a constellation of guide beacons, lasers, or natural stars that surround the target of interest. The same approach is used in AO for solar astronomy, except here a number of small regions of the solar surface that contain significant high spatial frequency information at appreciable contrast (e.g., sunspots, plage) replace the guide stars as beacons [1,2]. Each region is projected onto a Shack–Hartmann WFS that forms a set of images as observed through the sensor's subapertures. The images are each cross-correlated with a reference image and the local wavefront phase gradients obtained from the positions of the peak values.

As presently practiced, tomographic wavefront sensing can be thought of as a two-step process. [3–5]. To begin, line integrals of a quantity closely related to the atmospheric aberration, such as its first spatial derivative, are measured by the WFS along a number of discrete lines of sight. A tomographic algorithm then remaps the integrands onto horizontal layers defined at discrete altitudes in the atmosphere. The mapping is typically constrained to minimize the mean-square difference between the measured quantities and the corresponding estimates of the line integrals projected through the atmospheric model [6].

Our approach departs somewhat from this paradigm. We show in this Letter that tomographic wavefront information can also be recovered from a single beacon provided that its tracking rate is not constant. This will generally not be the case for astronomical observations but frequently will be when the objects are orbiting manmade satellites.

Instead of relying on multiple sight lines through the turbulent atmosphere, we exploit the fact that the aberration is strongly correlated on short time scales. We use the frozen flow model (FFM), which treats the evolution of the aberration as a series of independent static layers, each moving across the telescope aperture with the prevailing wind at the altitude of the layer. Because of its simplicity, the FFM is frequently used as the basis for numerical studies of telescope imaging performance, particularly in the modeling of AO systems. While the FFM is observed not to hold in the real world over long time scales, a number of studies [7–9] have shown that it is a reasonable approximation for short but still interesting periods. For example, from observations made at the 1.5 m telescope of the Starfire Optical Range in New Mexico, at 0.74 μm wavelength, Schöck and Spillar [9] found that the FFM is a good approximation for a time scale τ_{FFM} of 20 ms or less. The accuracy degraded over time such that after 100 ms only 50%

of the temporal evolution of the wavefront could be described by the FFM. Nevertheless, the period of validity of the model, τ_{FFM}, is an order of magnitude longer than τ_0, the expectation value of the time required for the phase of a wavefront in a circular telescope aperture to change by 1 rad rms [10].

In the very simple and artificial case of aberration characterized by a single frozen but wind-blown layer, it is easy to see that taking WFS data at two different times along the same line of sight can yield tomographic information in the same way as two simultaneous measurements along different lines of sight. The equivalent angular separation of the sight lines θ_s in the former case is $v_l t_{\mathrm{WFS}}/h_l$, where the quantities are, respectively, the wind speed v_l at the layer, the elapsed time t_{WFS} between frames of the WFS, and the range of the layer h_l from the telescope. In standard multibeacon tomography, θ_s is set by the geometry of the optical system and is known. However, in the single-beacon case, only t_{WFS} is known. To recover the same wavefront information, one must estimate both v_l and h_l.

Because we believe our method will be of most value in imaging artificial satellites, which often requires the use of a LGS, our analysis in the remainder of the Letter explores the case of a beacon at finite range. The result, however, is equally applicable to guide stars at any range. The geometry and nomenclature are established in Fig. 1.

We begin with an analysis of the WFS data to determine the number of layers of significant atmospheric aberration and their apparent velocity through the telescope's light path. The technique, described in detail by Hope *et al.* [11], relies on the 3D spatiotemporal autocorrelation of the wavefront slopes calculated from the signals of a Shack–Hartmann WFS. The signature of a frozen layer is a line of high correlation radiating from the origin. The angles made by the line with respect to the zero-spatial-lag axis in the autocorrelation cube are determined

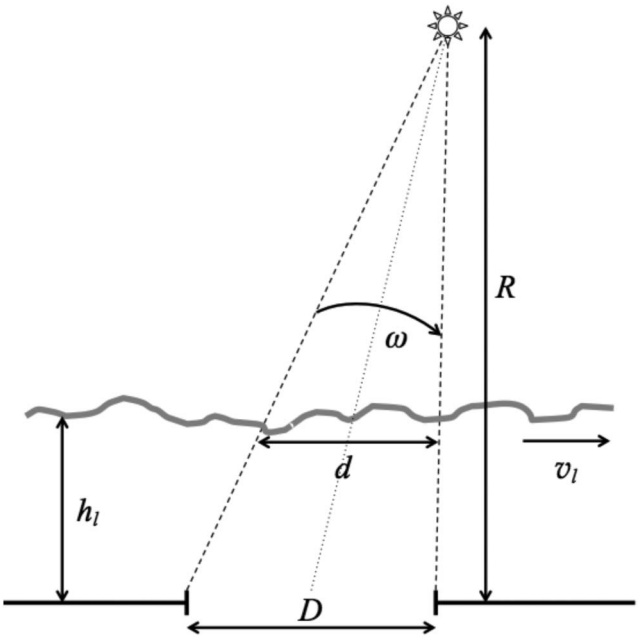

Fig. 1. Wavefront sensing geometry analyzed in this Letter. A LGS at range R illuminates a telescope of diameter D. A layer of atmospheric aberration at height h_l propagates with speed v_l. The LGS beam footprint at the layer has diameter d. The telescope tracks with angular speed ω.

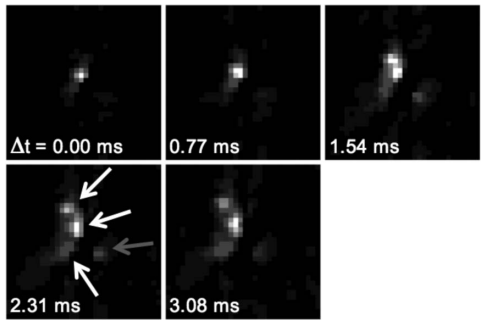

Fig. 2. Consecutive time-lag slices from the 3D autocorrelation of Shack–Hartmann WFS data. The three white arrows indicate correlation peaks corresponding to frozen aberration layers propagating with different velocities. The shaded arrow indicates a random peak not associated with a frozen layer.

by the apparent wind vector of the layer. The coherence time τ_{FFM} for the layer is estimated from the rate of decay of the correlation along the line, and although we do not use this information, the power in the line indicates the strength of the aberration. Figure 2 shows a number of consecutive time-lag slices from an autocorrelation cube calculated from WFS data recorded at the AEOS 3.6 m telescope in Hawaii. Peaks can be seen that correspond to three distinct layers above the telescope, as well as other peaks that do not lie on lines coming from the origin and reflect random correlations.

In the next step [11], we employ a nonlinear least-squares technique in a partial separation of the wavefront gradients on the layers we have identified. The estimates are constrained to match the WFS data in both space and time. Phases at each layer are then calculated from the gradients in the usual way. (Although not germane to tomography, the spatial subsampling afforded by the motion of each layer allows us to recover phase estimates on spatial scales shorter than the Nyquist limit imposed by the size of the WFS subapertures [12].)

We have built a small simulation to show this layer separation. Four atmospheric layers having different strengths, wind vectors, and heights were modeled with frozen Kolmogorov turbulence, as illustrated in Fig. 3. A sequence of 1000 phase screens in the pupil of a telescope of 4 m diameter was made by propagating the layers in time and light from a beacon through the layers. The beacon was taken to be at 90 km range, the approximate height of a sodium LGS. The WFS was modeled as a Shack–Hartmann with a grid of 32×32 subapertures

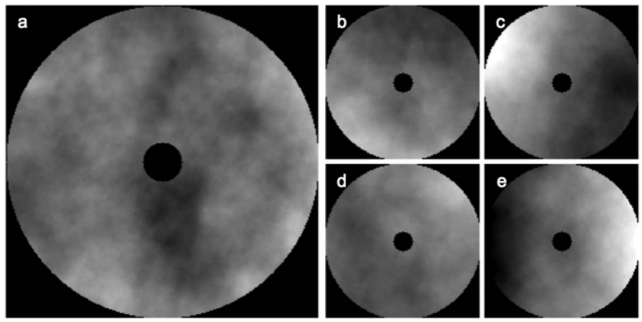

Fig. 3. Single frame from the atmospheric simulation. Combined aberration a is the sum of the four layers b through e.

Table 1. Parameters of the Model Atmosphere

Layer	r_0 (cm)[a]	Height (m)	Direction	Speed (ms^{-1})
1	17	0	0°	2
2	20	500	0°	10
3	30	5000	−10°	25
4	30	15000	40°	50

[a]Value of the Fried parameter at 500 nm wavelength.

running at 1300 frames per second. The parameters of the model atmosphere are listed in Table 1. The effective value of the Fried coherence length r_0 at 500 nm wavelength was 9.7 cm, and the coherence time τ_0 was 2.0 ms. The mean height of the aberration was 5400 m, giving an isoplanatic angle of 1.1 arc sec.

The effect of the layer separation is shown in Fig. 4, which compares the angular anisoplanatism as a function of field angle for two cases. In the first, all the aberration is taken to be in the telescope pupil, the conventional assumption for AO systems. In the second, the upper layer was separately estimated and taken to be at the correct range of 15 km. The lower three layers were estimated as a single layer, placed in the pupil.

At this point, although the short-term frozen flow character of the atmosphere has allowed us to determine the number of significant layers of aberration and to distinguish the detailed moment-by-moment contributions, we have still not established the layer ranges and cannot make use of our knowledge to mitigate either angular or focal anisoplanatism. The ranges are not uniquely constrained by the data. We can break the degeneracy, however, if observations can be made with the telescope tracking at two different angular velocities.

Referring to Fig. 1, we start by writing the time t_c for a point on a single layer to cross the telescope beam as

$$t_c = d/|\vec{v}_r|, \tag{1}$$

where superscript arrows represent vector quantities. The beam footprint diameter $d = D(1 - h_l/R)$ and the resultant velocity of the beam through the layer is given by

$$\vec{v}_r = \vec{v}_l - \vec{\omega} h_l. \tag{2}$$

Hence,

$$t_c = \frac{D(1 - h_l/R)}{(v_l^2 + \omega^2 h_l^2 - 2 v_l \omega h_l \cos A)^{1/2}}, \tag{3}$$

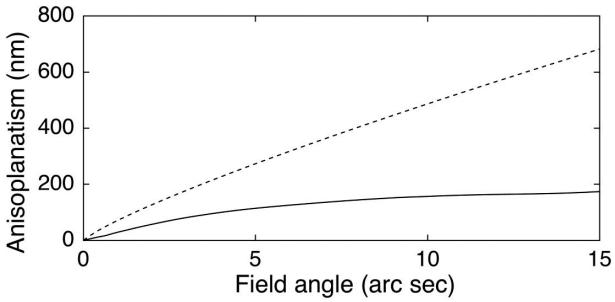

Fig. 4. Angular anisoplanatism for conventional wavefront compensation in the pupil plane only (dashed line) and for two altitude-conjugated correcting layers (solid line) applied to the modeled four-layer atmosphere.

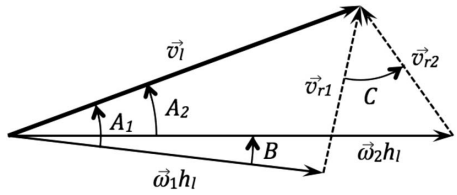

Fig. 5. Vector geometry of the apparent velocities $\vec{v}_r$ of the guide star footprint through a layer at height h_l moving with velocity $\vec{v}_l$ for two telescope track rates $\vec{\omega}_1$ and $\vec{\omega}_2$.

where A is the angle between the wind vector and the direction of motion of the beam induced by the telescope tracking.

The value of t_c for each layer is measured from the autocorrelation of the WFS data. However, there are three unknown quantities in Eq. (3): h_l, v_l, and A. A unique solution may be found from measurements of t_c with different values of $\vec{\omega}$, where the change in the angle of each layer's motion through the beam is also measured. That is, the tomographic problem can be fully solved if the telescope tracks at a nonconstant rate, provided that the layer ranges and velocities do not change significantly during the observations. This will naturally be the case for observations of most artificial satellites in nongeosynchronous orbits since the angular velocity of the telescope must vary to match the apparent track rate of the satellite across the sky.

The measurement geometry is illustrated in Fig. 5. Solving the triangles in terms of the known and measured quantities is quite straightforward and leads to a layer height

$$h_l = \left[\frac{\phi}{D} + \frac{1}{R}\right]^{-1}, \tag{4}$$

where

$$\phi = t_{c1} t_{c2} \left[\frac{\omega_1^2 + \omega_2^2 - 2\omega_1\omega_2 \cos(B)}{t_{c1}^2 + t_{c2}^2 - 2 t_{c1} t_{c2} \cos(C)}\right]^{1/2}. \tag{5}$$

Finding the actual layer velocities $\vec{v}_l$, if needed, is equally straightforward. It is worth noting that for $R \gg h_l$, the estimate of h_l is quite insensitive to changes in R, as may occur through changes in the mean height of the sodium layer.

We have tested the estimation of layer heights using our four-layer simulation. We assumed telescope tracking rates $\vec{\omega}_1$ and $\vec{\omega}_2$ of 0.2° s^{-1} and 0.4° s^{-1}, respectively, typical for low Earth-orbit satellites, with a 10° difference in direction. The apparent layer velocities and crossing times were determined by the autocorrelation algorithm from our simulated Shack–Hartmann WFS data. The actual and measured values of the crossing times and orientation shift (angle C in Fig. 5) are given in Table 2. The recovered estimates of the layer heights and velocities are shown in Table 3. These are to be compared with the true values in Table 1.

Table 2. Actual (*Measured*) Values of Apparent Layer Wind Vectors in Simulation

Layer	C (°)	t_{c1} (ms)	t_{c2} (ms)
1	0.0 (*0.1*)	2000 (*1620*)	2000 (*1818*)
2	−5.3 (*−0.7*)	482 (*470*)	604 (*690*)
3	−102.0 (*−104.2*)	451 (*481*)	265 (*276*)
4	54.2 (*54.3*)	95 (*96*)	50 (*52*)

Table 3. Results of the Layer Parameter Estimation

Layer	Height (m)	Direction (°)	Speed (ms^{-1})
1	74	1.2	2.7
2	750	2.1	11.0
3	4850	−9.5	24.0
4	14700	40.4	49.4

In the case of a satellite tracked with a LGS, our goal is to reduce the effects of focal anisoplanatism. This error term comprises three components: aberration at ranges beyond the beacon, unsensed aberration outside the cone defined by beacon light but encountered by light from the more distant object, and radial magnification of the sensed aberration as the beacon cone expands to fill the pupil. Our method does not address the first of these, which in any case is likely to be negligible, but the remaining two may be mitigated by, respectively, exploiting the FFM and our knowledge of the heights of significant layers.

Several methods have been suggested to take advantage of temporal coherence [13–15], including frozen flow characteristics, for improved wavefront control in AO systems. Here, the FFM allows us essentially to know the atmospheric aberration just outside the beacon light cone even when we cannot directly see it. Of course, we can only estimate aberration actually swept out by the beam footprint; some never will be, as illustrated in Fig. 6. Furthermore, in a closed-loop AO system, we can only know past history: the aberration that has already been sampled by the beacon and is now downstream. In that case, we may benefit from pointing the laser slightly away from the object along a direction parallel to $\vec{v}_r$ for the dominant high-altitude layer. In contrast, postprocessing applications such as deconvolution from wavefront sensing can take advantage of both future and past history, as we have shown with data taken at the 3.6 m AEOS telescope [11].

By placing the separated layers at their correct ranges, the beam compression ratio h_l/R can be taken into account in deriving the best estimate of the aberration: the radial magnification arising from the cone effect can be removed. The quantitative reduction in anisoplanatic effects achievable in this way will depend on the prevailing turbulence profile and the extent to which multilayer frozen flow behavior can account for the short-term evolution of the wavefront. For our model atmosphere in Table 1, the value of the focal anisoplanatism parameter d_0 is 1.9 m [16]. The error itself, given by $\lambda/2\pi(D/d_0)^{5/6}$, is 148 nm rms for our 4 m telescope, in satisfactory agreement with the value of 146 nm calculated directly from the 1000 composite phase screens of the simulation. We have computed the reduction in the error from our simulation by exploiting the layer separation illustrated in Figure 4 and the layer characteristics calculated from tomography in Table 3 to estimate the object phase in regions A, B, and C of Fig. 6. We also explicitly estimate the unsensed portions of the object wavefront (region D) via a set of 42 disk harmonic modes [17] extending over the full object footprint but fitted only to the estimated wavefront within the LGS footprint. In this way, the focal anisoplanatism is reduced by a factor of almost three to 54 nm rms.

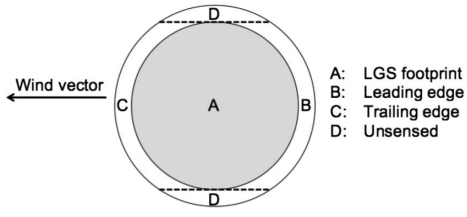

Fig. 6. Beam footprint of the object light (outer circle) on a high-altitude layer is only partially sampled by the LGS (shaded region A) at any given moment. The regions labeled D are never sampled.

This result is likely somewhat optimistic since the real atmosphere is not characterized by perfect frozen flow behavior, which we rely on to estimate the phase in regions B and C. For realistic wind speeds and a LGS at 90 km, however, the crossing time for these regions is of the order of milliseconds, an order of magnitude shorter than τ_{FFM}.

Focus anisoplanatism typically dominates the wavefront error budget for single-LGS AO systems. We expect that our method, where applicable, will reduce the effect of the error term to the point where that is no longer the case.

Even given the limitation that the FFM only allows phase estimation to be extended in the direction of each layer's wind vector, mitigation of angular anisoplanatism will be possible as well by placing the optical entrance pupil at some axial distance from the telescope and slightly reducing its size [18]. In this way, the footprint of light from objects at infinity can be arranged to stay within the sensed regions on all significant layers of aberration over a field of view roughly an order of magnitude larger than the isoplanatic angle.

Funding. Air Force Office of Scientific Research (AFOSR) (FA9550-14-1-0178).

REFERENCES

1. T. Rimmele, S. Hegwer, K. Richards, F. Wöger, J. Marino, D. Schmidt, and T. Waldmann, in *Proceedings of the Advanced Maui Optical and Space Surveillance Technologies Conference* (2008), paper E18.
2. G. Moretto, M. Langlois, P. Goode, N. Gorceix, and S. Shumko, in *Proceedings of the Third AO4ELT Conference* (2013), p. 106.
3. M. Lloyd-Hart, C. Baranec, N. M. Milton, M. Snyder, T. Stalcup, and J. R. P. Angel, Opt. Express **14**, 7541 (2006).
4. J. Marino and F. Wöger, Appl. Opt. **53**, 685 (2014).
5. M. Tallon and R. Foy, Astron. Astrophys. **235**, 549 (1990).
6. F. J. Rigaut, B. L. Ellerbroek, and R. Flicker, Proc. SPIE **4007**, 1022 (2000).
7. L. A. Poyneer, M. van Dam, and J.-P. Véran, J. Opt. Soc. Am. A **26**, 833 (2009).
8. E. Gendron and P. Léna, Astrophys. Space Sci. **239**, 221 (1996).
9. M. Schöck and E. J. Spillar, J. Opt. Soc. Am. A **17**, 1650 (2000).
10. D. L. Fried, J. Opt. Soc. Am. A **7**, 1224 (1990).
11. D. A. Hope, M. Hart, S. M. Jefferies, and J. G. Nagy, in *Advanced Maui Optical and Space Surveillance Technologies Conference* (2012), paper E51.
12. S. M. Jefferies and M. Hart, Opt. Express **19**, 1975 (2011).
13. K. Hinnen, M. Verhagen, and N. Doelman, J. Opt. Soc. Am. A **24**, 1714 (2007).
14. L. Poyneer and J.-P. Véran, J. Opt. Soc. Am. A **25**, 1486 (2008).
15. D. J. Goorskey, J. Schmidt, and M. R. Whiteley, Opt. Eng. **52**, 071418 (2013).
16. J. F. Belsher and D. L. Fried, "Expected antenna gain when correcting tilt-free wavefronts," Technical Report TR-576 (Optical Sciences Company, 1984).
17. N. M. Milton and M. Lloyd-Hart, *Adaptive Optics: Methods, Analysis and Applications* (Optical Society of America, 2005).
18. M. Lloyd-Hart, Opt. Lett. **27**, 1469 (2002).